Nanostructuring of Iron Surfaces by Low-Energy Helium Ions

İrem Tanyeli[1], Laurent Marot[2], Mauritius C.M. van de Sanden[1], Gregory De Temmerman[1]*

[1]FOM-Institute DIFFER, Dutch Institute For Fundamental Energy Research, Edisonbaan 14, 3439MN, Nieuwegein, The Netherlands

[2]Department of Physics, University of Basel, Klingelbergstrasse 82, Basel, Switzerland

KEYWORDS: Surface modification, iron, He-ion plasma

ABSTRACT The behavior of iron surfaces under helium plasma exposure is investigated as a function of surface temperature, plasma exposure time and He ion flux. Different surface morphologies are observed for large process parameter range and discussed in terms of temperature related surface mechanisms. Surface modification is observed under low He ion flux (in the range of 10^{20} $m^{-2}s^{-1}$) irradiation, whereas fiber like iron nanostructures are formed by exposing the surface to high flux (in the range of 10^{23} $m^{-2}s^{-1}$) of low energy He ions at surface temperatures of 450-700 °C. The effects of surface temperature and plasma exposure time on nanostructures are studied. The results show that surface processing by high flux low energy He ion bombardment provides a size controlled nanostructuring on iron surfaces.

INTRODUCTION

Nano-scaled materials provide an enhanced activity by their high surface area to volume ratios in various applications, especially in light driven processes. For instance, the efficiency of direct solar water splitting in photoelectrochemical cells is increased by nanostructuring the surface of metal oxides, which are used as photo electrodes.[1,2] Since the metal oxides suffer from the mismatch between light absorption depth and diffusion length of photogenerated charge carriers and also from the slow surface reaction kinetics, nanostructuring the surface is essential to overcome these drawbacks. In addition, black metals, which have high absorption over a large portion of the solar spectrum, are good candidates in solar thermal and solar thermo-photovoltaic systems.[3-5] Hence, there has been a paramount interest on the development of efficient nanostructuring methods in recent decades. The majority of these methods are wet chemistry methods, such as spray pyrolysis techniques and solution based colloidal methods, etc..[6,7] and competing in different aspects, such as time effectiveness, structure uniformities and size limitations.

Concerning the disadvantages of wet chemistry methods, ion assisted techniques have a great potential in nanostructuring metal surfaces as being dry processes. Micro-structural changes on metals induced by high energy (in the range of keV) ion bombardment have long been reported.[8,9] Irradiation by ions with energies above the threshold energy for displacement damage leads to radiation damages underneath the metal surface by formation of interstitials and vacancies. However, recent studies showed that radiation induced surface modifications can be obtained even with low energy (<50 eV) helium ion irradiation.[10,11] It is claimed that once helium atoms diffuse beneath the metal surface, they tend to agglomerate and form bubbles.[12] These helium bubbles coalesce and hereby they swell.[12] As a consequence of that nanostructures are formed by extending

the metal surface. Experimental studies showed that nanostructure formation is highly dependent on incident ion energy,[13] surface temperature[12] and ion flux.[14] Although the process is not fully understood and explained yet, a more detailed hypothesis on the formation process of helium-induced nanostructures can be found in.[12,15] Most of the experimental and theoretical studies have been conducted on tungsten.[16-18] The porosity of tungsten surfaces after helium plasma exposure reaches up to 90%, which implies a very high light absorption, almost 99% across the whole visible spectrum.[19] Similar helium induced morphology changes were observed on different metal surfaces, such as molybdenum, titanium and iron.[11,20] It was recently demonstrated that helium plasma processing of tungsten followed by a 2-step oxidation procedure allowed the formation of porous tungsten oxide with good photo-catalytic activity.[21] This demonstrates the potential of helium-ion irradiation for surface nanostructuring.

There has been a growing interest on the iron oxide photoanodes in photoelectrochemical water splitting.[1] Iron(III) oxide provides higher light absorption, namely higher solar to hydrogen (STH) conversion efficiency, than the other competing metal oxides, such as WO_3, TiO_2 due to its smaller bandgap.[1] In addition to that, its stability in aqueous environments and low cost make it a promising material for solar hydrogen production. However, the efficiency is limited by the poor charge carrier transport in iron oxide,[1] thus the surface needs to be nanostructured. Our study provides a controllable nanostructure formation on iron surfaces with surface temperature and plasma exposure time. After oxidation, these structures can be used as photo anodes for solar water splitting. All the processes starting from nanostructuring a mirror finish polished surface under high flux of low energy He ion irradiation to oxidizing to the desired oxide phase for solar water splitting have been demonstrated in principle for tungsten.[21]

In this study, we study the bottom up nanostructuring of iron surfaces by exposure to helium plasma. Helium-induced modifications of iron surface has recently been studied by Kajita *et al.*.[20] However, in this study we present a detailed investigation on the surface modification of iron under a large parameter range and as a mean to develop a controlled nanostructure growth. Iron surfaces were irradiated using two different flux regimes and within a broad temperature range for different plasma exposure times. In the present article the effect of these parameters on surface modification will be discussed.

EXPERIMENTAL

Polycrystalline iron samples (99.8% purity, Good Fellow) were exposed to helium plasma within a large range of ion fluxes ($1x10^{20}$ – $6.5x10^{23}$ $m^{-2}s^{-1}$). High flux irradiations were done in the Pilot-PSI linear plasma generator (Figure 1). The plasma is generated by a cascaded arc source which exhausts into a 50 cm diameter vacuum vessel. The plasma jet is confined by an axial magnetic field. The detailed description of setup can be found elsewhere.[22]

The magnetic field was set to 0.2 T during the experiments. Typical radial profiles of the electron temperature (T_e) and density (n_e) of the plasma beam, as measured by Thomson Scattering (TS) at 17 mm in front of the target, are shown in Figure 2. The plasma beam has a Gaussian shape and the maximum ion flux during exposures was in the range of $3.7\text{-}6.5x10^{23}$ $m^{-2}s^{-1}$. The samples are fixed onto a water-cooled target holder using a clamping ring made out of molybdenum (Mo), the distance between the plasma source and the sample surface is 54 cm. A layer of Grafoil® is inserted between the holder and the sample to provide a better thermal contact. The surface heating is induced by the incoming plasma flux and the surface temperature is regulated by water cooling. The samples are negatively biased with respect to the plasma potential to control the ion energy, which is set to 25 eV during the exposures.

Polycrystalline iron samples, which are 19 mm in diameter and 1 mm thick, were cut from a rod. These samples were mechanically polished with 320 to 2400 grit SiC papers and finalized to mirror finish by 3 to 1 μm diamond and 0.05 μm alumina suspensions. Polished samples were cleaned with acetone, ethanol and de-ionized water in ultrasonic bath, respectively while the acetone step was repeated at the end to easily remove the remaining water droplets on the surfaces. The diameter of the plasma-exposed area of the samples is larger than the FWHM of the beam, which is around 15 mm. Hence, the surface temperature profile has a Gaussian shape. The peak temperature was measured by a multiwavelength pyrometer (FMPI SpectroPyrometer, FAR Associates), which measures in the wavelength range of 900–1600 nm. In addition, the 2D surface temperature profile was measured by an infrared camera (FLIR A645 sc). The surface emissivity was determined by cross calibrating the measurements from both the pyrometer and the IR camera. The surface is modified by ions during the plasma exposure; hence the emissivity value changes. The emissivity of iron was found to be 0.19 at the beginning of exposure, and changed to 0.22 at the end of the exposure for a surface temperatures of around 450 °C and when the surface temperature reached to 700 °C, the emissivity increased to 0.26.

Low ion flux exposures were performed in an expanding thermal plasma setup called nano-PSI (Figure 1b).[23] Similar to Pilot-PSI, a cascaded arc source is used to generate the plasma, which is freely expanding into a spherical vessel with diameter of approximately 50 cm. The sample holder is positioned in the center of the spherical vessel; the diameter of the expanding plasma is larger than the diameter of the sample surface. This implies that there is no need to consider a spatial gradient for the ion flux or surface temperature. The sample can be actively heated up or water cooled so that the sample temperature is varied independently from the incident plasma flux. The sample temperature is measured by a K-type thermocouple, which is inserted through a hole at the

side of sample. Similarly to what is done in Pilot-PSI, the ion energy is set to 25 eV by applying a negative bias potential to the samples. A double Langmuir probe, which is 0.25 mm in diameter and 13.5 mm in length, is used to determine T_e and n_e. The measurements gave $T_e \sim 0.3$ eV and $n_e \sim 3.7 \times 10^{17} m^{-3}$. The ion flux is calculated to be about 1.3×10^{20} $m^{-2}s^{-1}$ at the beam center and the beam FWHM was measured to be about 5 cm i.e. much larger than the sample diameter.

After plasma exposures, the samples were analyzed by high-resolution scanning electron microscopy (SEM) to investigate the surface morphology changes and by X-ray photoelectron spectroscopy (XPS) to study the surface composition.

RESULTS AND DISCUSSION

Figure 3a and Figure 3b show the surface modifications on iron samples after high flux (3-4×10^{23} $m^{-2}s^{-1}$) He ion irradiation, with surface temperature of 130 °C for 5 minutes and 200 °C for 20 minutes, respectively. Ripples with a height of 3-10 nm, as was measured by AFM (Figure 3c), are observed on these surfaces. The ions hit the surface with an energy of 25 eV, which is slightly above the sputtering threshold energy for iron by He ions (≈ 24.22 eV).[25] The ripple orientation appears to depend on the grain orientation. In that sense, the formation of such structures is consistent with the Bradley Harper's model,[26] which is based on Sigmund's sputtering theory.[27] Moreover, the contribution from sputtering by impurities cannot be neglected. Some experimental studies reported that ripple formation is aided by destabilization of the surface by sputter co-deposition of impurity materials.[28,29] From XPS analysis, we have detected some traces of molybdenum in the region where we observe ripples. The most possible candidate for the source of Mo contamination in our experimental setup is the clamping ring. Although the sputtering threshold energy for Mo by He ions (≈ 59 eV) is quite above the energy imposed by biasing in our case,[25] the enhancement in the localized electric field around the sharp regions of our clamping

ring could cause sputtering. It should be noted that surface modifications by the formation of a wavy-structure has been reported for the case of tungsten surfaces after irradiation by high flux of low energy He ions with energies below the sputtering threshold of tungsten.[24] Those structures were accompanied by the formation of pinholes on the surface and it is not entirely clear that the same process is occurring in the case of iron where pinholes cannot be observed. It is worthy to note that, in the present case, these structures are not observed at the location of the highest heat flux (Figure 3d), but they are found at 5-6 mm away from the beam center, i.e. almost at the edge of the plasma beam. Vasiliu *et al.* observed a similar situation on iron samples irradiated by high energetic (in keV range) Ar ions.[30] They claimed that there is a defect and dislocation flow from the center of the beam to the edge where temperature and ion flux gradients exist.

Figure 4a and Figure 4b show SEM images of iron samples exposed to He plasma with flux of 3.5×10^{23} $m^{-2}s^{-1}$ at surface temperatures of 270 °C and 450 °C, respectively. The ripples, which we observe up to a surface temperature of 200 °C, disappear and no periodic or continuous structures exist on the surface. At a surface temperature of 450 °C, some holes begin to appear on the surface as shown in Figure 4b. Organized helium induced nanostructure formation starts above 450 °C and fiber-like nanostructures are observed up to 700 °C. Iron surfaces after helium plasma exposure with the ion flux of $3.5\text{-}6.5 \times 10^{23}$ $m^{-2}s^{-1}$ in that temperature range are shown in Figure 5. As shown in the first SEM images of each row in Figure 5, a network like structure is observed on the surface. With the increase in the surface temperature, nano-sized structures appear on the surface. Once these structures form, their characteristic size increases with temperature. The individual structure size for 5 minute exposure with surface temperature of 570 °C is around 100-200 nm in diameter, whereas for longer exposures the nanostructures become finer with a diameter around 50-100 nm. To get a quantitative insight on how the size of nanostructures is affected by the surface

temperature and exposure time, SEM images in Figure 5 were analyzed using the Gwyddion software.[31] Since the structures are randomly shaped, instead of a mean diameter, the mean grain area was plotted against surface temperature for three different exposure times in Figure 6. The mean grain area covered by iron nanostructures increases with surface temperature for all three different plasma exposure times. It is also worthy to point out that the individual structure sizes and mean grain areas of iron nanostructures formed under plasma irradiation with surface temperatures of around 700 °C for both 20 and 60 minute exposures are very close to each other, namely the structures seem not to evolve further after 20 minutes exposure. With further increase in temperature we could mention that re-crystallization might affect the mechanisms for surface modification as seen in Figure 4c and Figure 4d, i.e. for surfaces exposed to a surface temperature above 780 °C. For pure iron, re-crystallization temperature is around 450 °C, a temperature which can be higher for less pure iron grades.[32]

We already observed the upper limit of He ion fluence for nanostructure formation as shown in Figure 5. To investigate the lower boundary for He induced surface modification, iron surfaces were exposed to low flux of He ions, in the order of 10^{20} $m^{-2}s^{-1}$. The surface temperature was set to 300 °C, where nanostructuring is not observed on samples exposed in the high flux regime (see Figure 4), and to 600 °C, where fine nanostructures form under high ion flux irradiation (see Figure 5). The iron surfaces exposed with surface temperatures of 300 °C and 600 °C for 1 hour in nano-PSI are shown in Figure 7. The surfaces at both temperatures are affected by plasma irradiation. Instead of fine nanostructures, we observe random nanostructures on both iron surfaces which were exposed at 300 °C and 600 °C. The nanostructure growth from the surface, for tungsten and molybdenum, is attributed to the formation of pressurized bubbles,[34] and a sufficient ion fluence is needed. In general, our exposures on iron samples from different flux regimes indicate that there

is a threshold He ion fluence to have He ion induced nanostructure growth on iron. Similarly but more extensively, the effects of ion energy[12] and ion flux[14] on growth kinetics of the nanostructured layer on tungsten surface have been reported.

Figure 4 and Figure 5 revealed that there is a strong correlation between the surface temperature, ion fluence and the surface modification. During the nanostructure formation different mechanisms take place, such as ion erosion, helium ion diffusion, surface diffusion, volume viscous flow, void formation, re-crystallization. One or several of these competing mechanisms become dominant depending upon the temperature range and ion fluence. The formation of ripples indicated that the ion erosion may be a process in the low temperature range, around 150-200 °C in our experiments (Figure 3). Moreover, with the increase in temperature, the mechanisms, which are temperature driven, may become predominant. For instance, the surface diffusion becomes more rapid. The temperature dependence of self diffusion coefficients in bcc Fe was plotted starting from 227 °C in the study of Mendelev and Mishin.[35] They showed that it follows an Arrhenius type behavior. With increase in temperature the surface kinetics may be taken over by surface smoothing which is driven by the reduction of surface energy. Beyond 450 °C a well organized surface modification starts to be observed (Figure 5). When the surface temperature is further increased; nanostructures with a diameter of 100-200 nm tend to grow from the surface. These structures were analyzed by TEM to gain more insight on their inner structure. As seen in Figure 9, pores are detected in the near-surface with sizes lower than 20 nm. Similarly, in the cross section view of the structures shown in Figure 9a, pores are visualized. Pinholes can be observed for different parts of the surface (Figure 9b) which are exposed to different ion fluxes because of the Gaussian plasma profile. For tungsten it was shown that pinholes are formed at the earlier

stages of nanostructure formation under He ion irradiation[36] and precede the formation of the rod-like structure.

The force by pressurized He bubbles leads a viscous flow of metal from the surface.[15] Once these structures form, they enlarge with temperature. Stewart *et al.* simulated the formation and diffusion of He clusters and bubbles in iron for temperatures up to 927 °C.[37] They showed that the diffusion rate of Helium interstitials and clusters increases with temperature. As a consequence of that, helium bubbles coalesce rapidly and this leads to larger sized features. We observe a similar trend in our experimental results. The presence of voids underneath the surface indicates that there is a similarity in nanostructure formation on iron, tungsten and molybdenum surfaces- all three are bcc metals. However, the thickness of the nanostructured layer was found to be around 500 nm, which is much less than what is typically observed on tungsten or molybdenum under similar exposure times. The nanostructured layer thickness on tungsten surfaces, which were exposed at 1000 °C, 1500 °C and 2000 °C for 500 and 1000 s, was around 1-2 μm.[11] This implies that, there has to be another process which limits the nanostructured layer growth on iron. When we consider our experimental conditions, the most likely candidate which could decelerate the growth process on iron surface seems to be physical sputtering. The effect of physical sputtering on the nanostructured layer growth on tungsten surface was studied by Doerner *et al.* by bombarding the surface at different incident ion energies.[18] No net erosion yield was detected after the exposures at energy well below the threshold for physical sputtering of tungsten by helium; hence the growth rate of nanostructured layer revealed its inverse square root of time dependence as shown in one of their previous studies.[16] They achieved a stationary nanostructured layer thickness under higher energetic ion irradiation due to the fact that the growth rate and sputtering rate compete and reach a balance. The ion energy in our study is slightly above the threshold energy for iron sputtering by

helium ions. Hence, we can expect to observe sputtering on iron surface whereas the effect of sputtering is negligible in the tungsten case. To verify that assumption, the mass of our samples was measured before and after plasma exposures. From those mass loss measurements, the sputtering yield (Y) can be calculated by

$$Y = \frac{\Delta m}{M_2 n_1} N_0 \quad (1)$$

where Δm is the mass change, M_2 the iron's atomic mass, n_1 number of He ions reaching the surface and N_o Avogadro's number. The plot of the measured sputtering yield versus ion fluence is seen in Figure 10. The general trend in sputtering yield is decreasing with ion fluence and it reaches a steady state regime for ion fluencies higher than $3x10^{26}$ m^{-2}. Nishijima *et al.* bombarded their nanostructured tungsten surfaces by Ar ions.[38] In that study, they detected a clear reduction in the sputtering yield of porous surface compared to the yield measured from smooth surface. Consistently with that, in our case the end of rapid decrease in the sputtering yield corresponds to the region where we obtain nanostructured surfaces with a porous surface. In general, it can be noted that the dependency of the nanostructure growth kinetics on surface temperature and plasma exposure time for iron surfaces is consistent with the results from tungsten and molybdenum surfaces[11] which might indicate that a similar mechanism is active.

To gain insight into the chemical composition of our samples, they were analyzed by XPS. The measurements were taken from polished iron surfaces before and after plasma exposure (Figure 11). Both unexposed and plasma exposed iron surfaces show elemental iron (Fe $2p_{1/2}$ and Fe $2p_{3/2}$ at binding energies of 719.9 eV and 706.8 eV, respectively) and iron oxide (Fe $2p_{1/2}$ and Fe $2p_{3/2}$ at binding energies of 724.6 eV and 710.9 eV, respectively) consistently with literature values.[39] Both samples show the expected ratio on Fe $2p_{3/2}$ vs. Fe $2p_{1/2}$ of 2:1. Figure 11 shows the iron oxide content to be bigger in the plasma exposed surface than in the unexposed one. Assuming on

the single overlayer model to quantify the iron oxide to iron elemental ratio, the exposed sample shows approximately twice the amount of iron oxide compared to the unexposed sample. The difference in the oxidation might be attributed to the increased surface area after plasma exposure, namely higher reactive area with oxygen. A significant contribution due to different morphologies cannot be excluded. Considering the slight shifts in the peak positions for our measurements and the reference article, the oxide phase on our samples is possibly a non-stoichiometric structure between Fe_2O_3 and Fe_3O_4. For applications in solar water-splitting, the Fe_2O_3 phase is desired and future work will concentrate on the development of stoichiometric oxides after nanostructuring by helium ions. A proof-of-principle of this approach has recently been reported by de Respinis *et al.*.[21]

CONCLUSION

The effect of helium plasma treatment of iron surfaces has been studied. A control over nanostructure formation is achieved by surface temperature and plasma exposure time. Pressurized helium bubble induced surface morphology changes are clearly observed under high flux (3-6.8x10^{23} $m^{-2}s^{-1}$) irradiations. A controlled nanostructure formation is achieved in between 450 °C and 700 °C. The nanostructures become larger with the increase in surface temperature and become finer with the plasma exposure time until they reach the saturation limit in ion fluence. Fine nanostructures, which are around 50 nm in diameter and 500 nm in length, are grown on iron surface after high flux of low energy He ions exposure at 700 °C for 20 minutes. Despite of some differences in nanostructure growth kinetics of iron and tungsten, the dependency of the feature size on surface temperature shows consistency indicating that the mechanisms of helium-induced modifications might be similar for those metals.

FIGURES

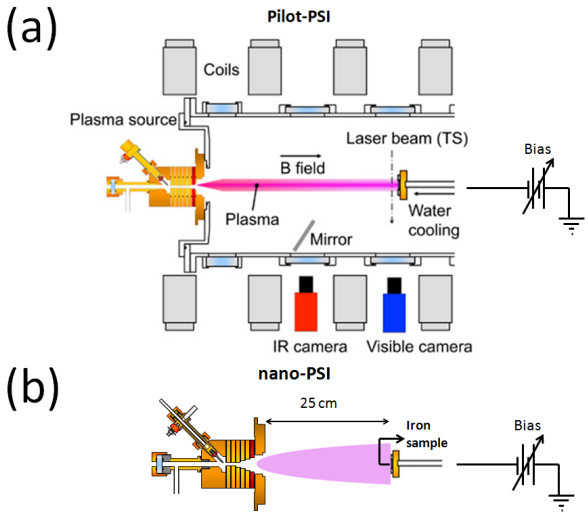

Figure 1. Schematic view of Pilot-PSI (a) and nano-PSI (b).

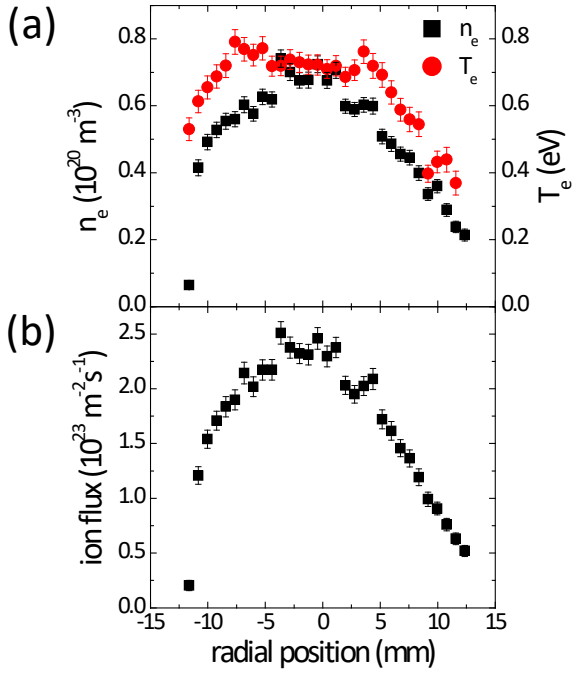

Figure 2. Electron density (n_e), temperature (T_e) (a) and ion flux density (b) profiles of the helium plasma beam in Pilot-PSI obtained from Thomson scattering.

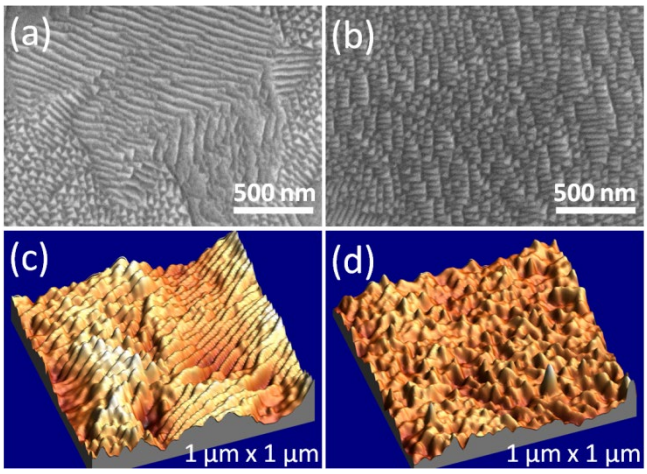

Figure 3. SEM images of iron surfaces exposed to He plasma (ion flux of 3-4x10^{23} $m^{-2}s^{-1}$) with surface temperature of 130 °C for 5 minutes (a) and 200 °C for 20 minutes (b), AFM images of iron surface exposed to He plasma with surface temperature of 130 °C for 5 minutes taken from 5-6 mm away from beam center (c) and from the beam center (d).

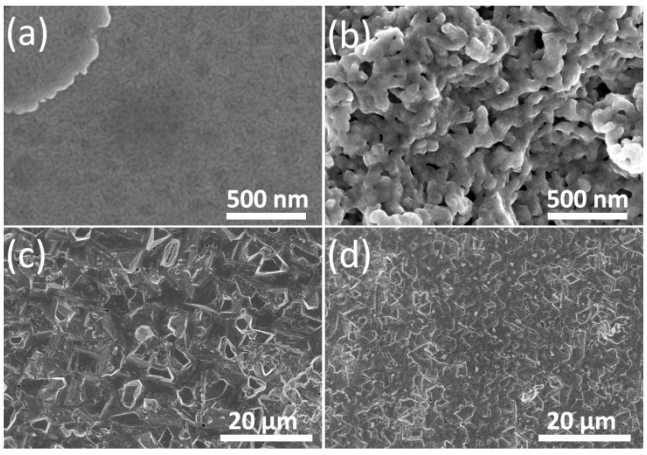

Figure 4. SEM images of iron surfaces after He plasma exposure at 270 °C (a), 450 °C (b), 780 °C (c) and 940 °C (d) with ion flux of 3.5x10^{23} $m^{-2}s^{-1}$.

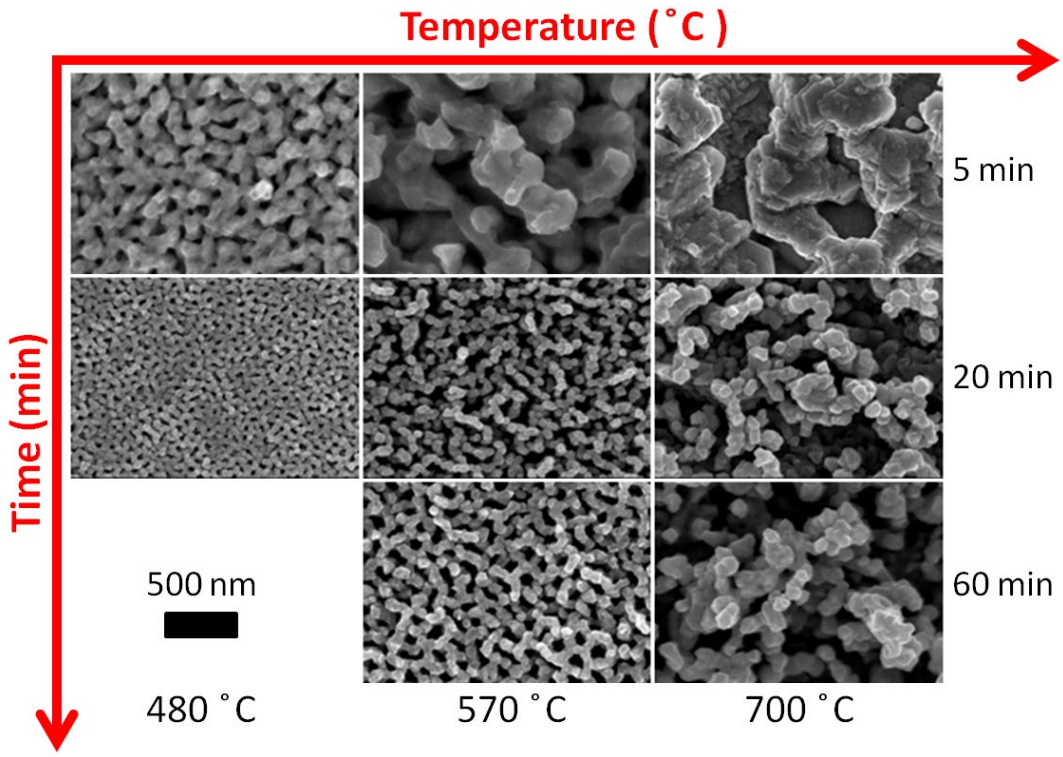

Figure 5. Evolution of He induced nanostructure formation on iron surface for three different exposure times with ion flux of 3.5-6.5x10^{23} $m^{-2}s^{-1}$.

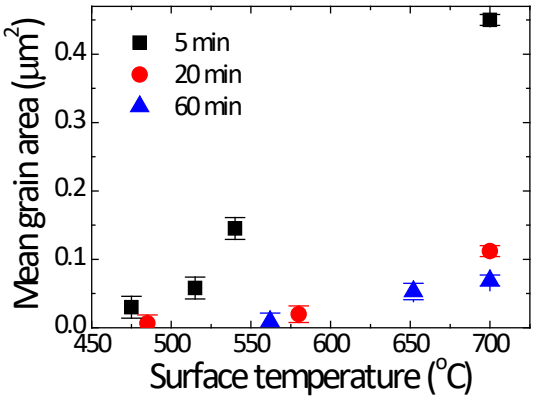

Figure 6. Mean grain area vs. surface temperature.

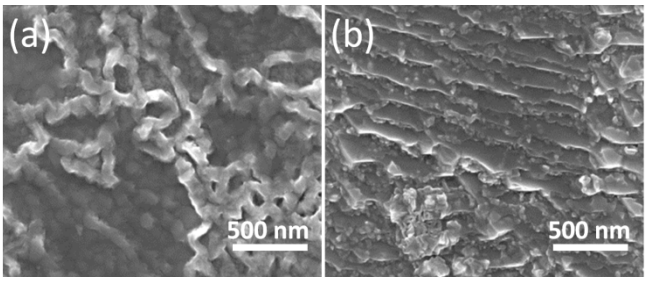

Figure 7. Surface modification of iron exposed to He fluence of 4.7×10^{23} m^{-2} (1 hour) with surface temperature of 300 °C (a) and 600 °C (b).

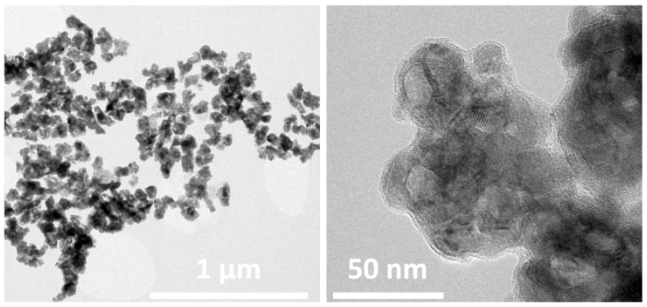

Figure 8. TEM images taken from nanostructures formed after plasma exposure at 700 °C for 20 minutes.

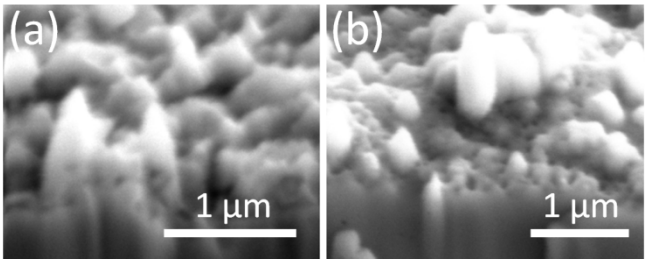

Figure 9. Pores are detected both inside of the nanostructures (a) and in the regions outer part of the beam center (b).

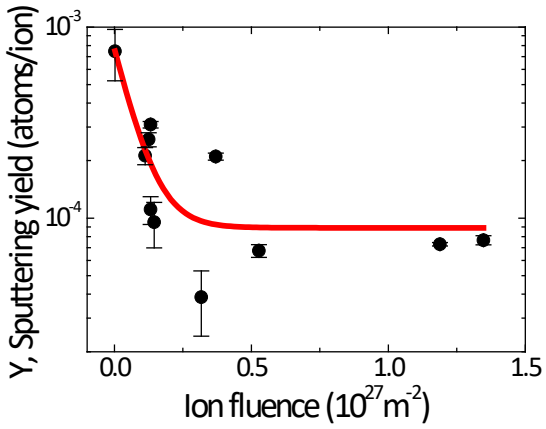

Figure 10. Sputtering yield versus ion fluence.

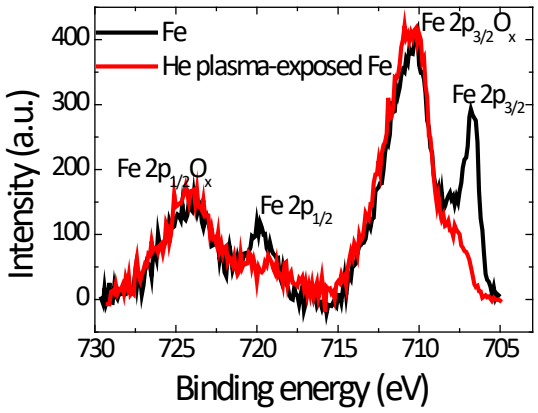

Figure 11. XPS of reference iron and plasma exposed iron.

AUTHOR INFORMATION

Corresponding Author

*Irem Tanyeli: i.tanyeli@differ.nl

ACKNOWLEDGMENT

The authors would like to thank Erwin Zoethout for XPS measurements and Osman El-Atwani for cross section images. This work is part of the research programme of the Stichting voor Fundamenteel Onderzoek der Materie (FOM), which is financially supported by the Nederlandse

Organisatie voor Wetenschappelijk Onderzoek (NWO). It is supported by the European Communities under the contract of Association between EURATOM and FOM and carried out within the framework of the European Fusion Programme.

REFERENCES

(1) Sivula, K.; Le Formal, F.; Grätzel, M. Solar Water Splitting: Progress Using Hematite (α-Fe_2O_3) Photoelectrodes. *ChemSusChem* **2011**, 4, 432 – 449.

(2) Berger, S.; Tsuchiya, H. ; Ghicov, A.; Schmuki, P. High photocurrent conversion efficiency in self-organized porous WO_3. *Appl. Phys. Lett.* **2006**, 88, 203119-1 – 203119-3.

(3) Nagpal, P.; Han, S. E.; Stein, A.; Norris, D. J. Efficient Low-Temperature Thermophotovoltaic Emitters from Metallic Photonic Crystals. *Nano Lett.* **2008**, 8 (10), 3238 – 3243.

(4) Rephaeli, E.; Fan, S. Tungsten black absorber for solar light with wide angular operation range. *Appl. Phys. Lett.* **2008**, 92, 211107-1 – 211107-3.

(5) Ungaro, C.; Gray, S. K.; Gupta, M. C. Black tungsten for solar power generation. *Appl. Phys. Lett.* **2013**, 103, 071105-1 – 071105-3.

(6) Duret, A.; Grätzel, M. Visible Light-Induced Water Oxidation on Mesoscopic α-Fe_2O_3 Films Made by Ultrasonic Spray Pyrolysis. *J. Phys. Chem. B* **2005**, 109 (36), 17184 – 17191.

(7) Brillet, J.; Grätzel, M.; Sivula, K. Decoupling Feature Size and Functionality in Solution-Processed, Porous Hematite Electrodes for Solar Water Splitting. *Nano Lett.* **2010**, 10 (10), 4155 – 4160.

(8) Sakamoto, R.; Muroga, T.; Yoshida, N. Microstructural evolution induced by low energy hydrogen ion irradiation in tungsten. *J. Nucl. Mater.* **1995**, 220 – 222, 819 – 822.

(9) Nakamura, Y.; Kitajima, S.; Shinohara, K. Influence of 100 keV helium irradiation on tensile properties of pure iron and JFMS steel at low temperatures. *J. Nucl. Mater.* **1989**, 169, 185 – 197.

(10) Tokunaga, K.; Baldwin, M. J.; Doerner, R. P.; Noda, N.; Kubota, Y.; Yoshida, N.; Sogabe, T.; Kato, T.; Schedler, B. Blister formation and deuterium retention on tungsten exposed to low energy and high flux deuterium plasma. *J. Nucl. Mater.* **2005**, 337 – 339, 887 – 891.

(11) De Temmerman, G.; Bystrov, K.; Zielinski, J. J.; Balden, M.; Matern, G.; Arnas, C.; Marot, L. Nanostructuring of molybdenum and tungsten surfaces by low-energy helium ions. *J. Vac. Sci. Technol., A* **2012**, 30, 041306-1 – 041306-6.

(12) Kajita, S.; Sakaguchi, W.; Ohno, N.; Yoshida, N.; Saeki, T. Formation process of tungsten nanostructure by the exposure to helium plasma under fusion relevant plasma conditions. *Nucl. Fusion* **2009**, 49, 095005-1 – 095005-6.

(13) Nishijima, D.; Ye, M. Y.; Ohno, N.; Takamura, S. Incident ion energy dependence of bubble formation on tungsten surface with low energy and high flux helium plasma irradiation. *J. Nucl. Mater.* **2003**, 313 – 316, 97 – 101.

(14) Baldwin, M. J.; Doerner, R. P.; Nishijima, D.; Tokunaga, K.; Ueda, Y. The effects of high fluence mixed-species (deuterium, helium, beryllium) plasma interactions with tungsten. *J. Nucl. Mater.* **2009**, 390–391, 886 – 890.

(15) Krasheninnikov, S. I. Viscoelastic model of tungsten 'fuzz' growth. *Phys. Scr.* **2011**, T145, 014040-1 – 014040-4.

(16) Baldwin, M. J.; Doerner, R. P. Helium induced nanoscopic morphology on tungsten under fusion relevant plasma conditions. *Nucl. Fusion* **2008**, 48, 035001-1 – 035001-5.

(17) Nishijima, D.; Iwakiri, H.; Amano, K.; Ye, M. Y.; Ohno, N.; Tokunaga, K.; Yoshida, N.; Takamura, S. Suppression of blister formation and deuterium retention on tungsten surface due to mechanical polishing and helium pre-exposure. *Nucl. Fusion* **2005**, 45, 669 – 674.

(18) Doerner, R. P.; Baldwin, M. J.; Stangeby, P. C. An equilibrium model for tungsten fuzz in an eroding plasma environment. *Nucl. Fusion* **2011**, 51**,** 043001-1 – 043001-6.

(19) Kajita, S.; Saeki, T.; Yoshida, N.; Ohno; N.; Iwamae, A. Nanostructured Black Metal: Novel Fabrication Method by Use of Self-Growing Helium Bubbles. *Appl. Phys. Express* **2010**, 3, 085204–1 – 085204–3.

(20) Kajita, S.; Yoshida, T.; Kitaoka, D.; Etoh, R.; Yajima, M.; Ohno, N.; Yoshida, H.; Yoshida, N.; Terao, Y. Helium plasma implantation on metals: Nanostructure formation and visible-light photocatalytic response. *J. Appl. Phys.* **2013**, 113, 134301-1 – 134301-7.

(21) de Respinis, M.; De Temmerman, G.; Tanyeli, I.; van de Sanden, M. C. M.; Doerner, R. P.; Baldwin, M. J.; van de Krol, R. Efficient plasma route to nanostructure materials: case study on the use of m-WO_3 for solar water splitting. *ACS Appl. Mater. Interfaces* **2013**, 5*,* 7621 – 7625.

(22) De Temmerman, G.; Zielinski, J. J.; van Diepen, S.; Marot, L.; Price, M. ELM simulation experiments on Pilot-PSI using simultaneous high flux plasma and transient heat/particle source. *Nucl. Fusion* **2011**, 51, 073008-1 – 073008-8.

(23) Bystrov, K.; Morgan, T. W.; Tanyeli, I.; De Temmerman, G.; van de Sanden, M. C. M. Chemical sputtering of graphite by low temperature nitrogen plasmas at various substrate temperatures and ion flux densities. *J. Appl. Phys.* **2013**, 114, 133301-1 – 133301-11.

(24) Ohno, N.; Hirahata, Y.; Yamagiwa, M.; Kajita, S.; Takagi, M.; Yoshida, N.; Yoshihara, R.; Tokunaga, T.; Tokitani, M. Influence of crystal orientation on damages of tungsten exposed to helium plasma. *J. Nucl. Mater.* **2013,** 438, S879 – S882.

(25) Eckstein, W. In *Sputtering by Particle Bombardment;* Behrisch, R., Eckstein, W., Eds.; Top. Appl. Phys., 110, Springer-Verlag: Berlin, 2007; Chapter - Sputtering Yields, pp 33 – 187.

(26) Bradley, R. M.; Harper, J. M. E. Theory of ripple topography induced by ion bombardment. *J. Vac. Sci. Technol., A* **1988**, 6, 2390 – 2395.

(27) Sigmund, P. Theory of Sputtering. I. Sputtering Yield of Amorphous and Polycrystalline Targets. *Phys. Rev.* **1969**, 184, 383 – 416.

(28) Macko, S.; Frost, F.; Ziberi, B.; Förster, D. F.; Michely, T. Is keV ion-induced pattern formation on Si(001) caused by metal impurities?. *Nanotechnology* **2010**, 21, 085301-1 – 085301-9.

(29) Özaydin, G.; Özcan, A. S.; Wang, Y.; Ludwig, K. F.; Zhou, H.; Headrick, R. L.; Siddons, D. P. Real-time x-ray studies of Mo-seeded Si nanodot formation during ion bombardment. *Appl. Phys. Lett.* **2005**, 87, 163104-1 – 163104-3.

(30) Vasiliu, F.; Teodorescu, I. A.; Glodeanu, F. SEM investigations of iron surface ion erosion as a function of specimen temperature and incidence angle. *J. Mater. Sci.* **1975**, 10, 399 – 405.

(31) Klapetek, P.; Nečas, D. Gwyddion, Czech Metrology Institute, **2007**, http://gwyddion.net.

(32) Bugayev, K.; Konovalov, Y.; Bychkov, Y.; Kovalenko, V.; Tretyakov, E. *Iron and Steel Production*, Books for Business: New York-Hong Kong, 2001.

(33) Evans, J. H. An interbubble fracture mechanism of blister formation on helium-irradiated metals. *J. Nucl. Mater.* **1977**, 68, 129 – 140.

(34) Kajita, S.; Nishijima, D.; Ohno, N.; Takamura, S. Reduction of laser power threshold for melting tungsten due to subsurface helium holes. *J. Appl. Phys.* **2006**, 100, 103304-1 – 103304-10.

(35) Mendelev, M. I.; Mishin, Y. Molecular dynamics study of self-diffusion in bcc Fe. *Phys. Rev. B* **2009,** 80, 144111-1 – 144111-9.

(36) Kajita, S.; Sakaguchi, W.; Ohno, N.; Yoshida, N.; Saeki, T. Formation process of tungsten nanostructure by the exposure to helium plasma under fusion relevant plasma conditions. *Nucl. Fusion* **2009**, 49, 095005-1 – 095005-6.

(37) Stewart, D.; Osetskiy, Y.; Stoller, R. Atomistic studies of formation and diffusion of helium clusters and bubbles in BCC iron. *J. Nucl. Mater.* **2011**, 417, 1110 – 1114.

(38) Nishijima, D.; Baldwin, M. J.; Doerner, R. P.; Yu, J. H. Sputtering properties of tungsten 'fuzzy' surfaces. *J. Nucl. Mater.* **2011**, 415, S96 – S99.

(39) Kim, K. J.; Moon, D. W.; Lee, S. K.; Jung, K. H. Formation of a highly oriented FeO thin film by phase transition of Fe_3O_4 and Fe nanocrystallines. *Thin Solid Films* **2000**, 360, 118 – 121.

For Table of Contents Only